J Sci Comput
DOI 10.1007/s10915-011-9567-2

Image Approximations to Electrostatic Potentials in Layered Electrolytes/Dielectrics and an Ion-Channel Model

Huimin Lin · Zhenli Xu · Huazhong Tang · Wei Cai

Received: 16 June 2011 / Revised: 24 November 2011 / Accepted: 5 December 2011

Abstract Image charge approximations are developed for electric potentials in the Poisson-Boltzmann theory in inhomogeneous media consisting of dielectrics or electrolyte solutions such as the layered structure in a membrane or cylindrical ion-channels. The image charges are obtained either by a least square fitting between the potential of unknown images and the exact reaction potential (for the layered media or cylindrical region) or by a Prony fitting to the Fourier transform of the exact potential (layered media only) and a Sommerfeld-type identity, which yields the locations and strengths of the image charges. Next, combining the results for the two geometries, the image charge approximation for the reaction potential, due to a charge inside an ion-channel model, is obtained, which accounts for the polarization of the region outside the ion-channel (consisting of a membrane and electrolyte solutions below and above). Such an approximation to the reaction field in the ion-channel model can be used for an explicit/implicit hybrid treatment of electrostatics interaction in modeling ion-channels. Numerical tests show that the proposed method has an attractive performance in computing electrostatic interactions of source charges inside the ion-channel model via a simple summation of pairwise interactions among source and image charges.

Keywords Poisson-Boltzmann equation · Layered electrolytes and dielectrics · Method of images · Ion channels · Hybrid explicit/implicit solvent models

H. Lin · H. Tang
HEDPS, CAPT & LMAM, School of Mathematical Sciences, Peking University, Beijing 100871, P.R. China

Z. Xu
Department of Mathematics, and Institute of Natural Sciences, Shanghai Jiao Tong University, Shanghai 200240, China

W. Cai (✉)
Department of Mathematics and Statistics, University of North Carolina at Charlotte, Charlotte, NC 28223, USA
e-mail: wcai@uncc.edu

W. Cai
Beijing International Center for Mathematical Research, Beijing 100871, China

Published online: 21 December 2011

1 Introduction

The electrostatic force is one of the most important forces in the structure and stability of biomolecules in an aqueous environment [1, 2]. The classical electrostatic theory applies to the medium comprised of solute macromolecules and surrounding solvent environment. The Poisson-Boltzmann (PB) theory [2–5] is based on a mean-field approximation [6], where the force on an ion is given by the ion charge times the macroscopic electric field of the solute-solvent system, the latter is given by the field of mean potential. The PB theory is successful in describing the electrostatic interaction of biological systems as long as the electrostatic coupling strength is weak. The linearized Poisson Boltzmann equation analyzed here has been used often to approximate ionic solutions [7]. We study the linearized PB equation here as its mathematical analysis and approximation by image methods is possible, which is difficult if not impossible for more realistic models. Unfortunately, many physical chemists have rejected both the nonlinear and linearized Poisson Boltzmann equation as a model of ionic solutions [8–11] as PB equations (nonlinear and linear) do not include the effects of steric repulsion between finite sized ions. This repulsion has dramatic effects on the behavior of ionic solutions, particularly of mixtures containing divalents. Almost all biological solutions are mixtures containing divalents. Also, it is widely known that the mean-field PB theory fails to describe interactions of crowded charges in ion channels as it ignores finite size effects and ion correlations [12–15]. Still, we hope the mathematical methods and insights developed here will lead to progress in the study of more realistic models of ionic solutions.

The description of solvents surrounding a solute or the membrane/solvents around an ion-channel can be either atomistic as in an explicit model or continuum as in an implicit model. The selection of a specific model for the solvent depends on the accuracy and efficiency desired for the simulation. In order to take advantage of the accuracy of the explicit model and the efficiency of the implicit PB model, hybrid explicit/implicit solvent models have been studied [16–22]. In such a model, the simulation system is partitioned into two regions. The inner region, usually of a regular geometric shape such as a sphere or a finite cylinder, containing the solute or the transmembrane channel under study, and a remaining region exterior to the sphere or the cylinder. In the former region, an atomistic description is used for the solute and the solvent molecules while in the latter region, the membrane/solvent is described by dielectric constants or Debye-Hückel length parameters, which reflect the salt concentration.

In the molecular dynamic simulation within the hybrid model, only the atoms inside the explicit region are dynamically simulated while the effect of the implicit region is included by the use of a reaction field from the polarization of the implicit solvent by the charges inside the explicit region. Therefore, it is important to have a fast and accurate method to calculate the reaction field for a given geometry of the explicit region. In the case of a sphere, the classical Kirkwood series expansion [23, 24] can be used to calculate the reaction field of point charges inside the spherical cavity. However, the Kirkwood expansion has a slow convergence rate, especially for charges close to the boundary of the cavity. The image charge methods [25–27] provide a simple alternative to calculate the reaction field efficiently. As the images are in Coulombic form, approximating the reaction field with discrete image charges will result in a linear scaling calculation once fast algorithms such as the fast multipole method [28–30] are utilized to speed up the particle interactions. Furthermore, multiple image methods [30–33] have been developed to provide an approximation with high order accuracy by increasing the number of images. Recent studies [21, 34] demonstrated the image methods are promising for the reaction-field calculations of spherical cavities once the FMM is incorporated. Similar methods of images have been applied to a cylinder [35],

which offers an efficient approximation to an exact series solution in terms of cylindrical harmonics [36], where image charges are obtained through a least square optimization process. It should be mentioned that the dielectric interface has been studied intensively in the context of ion-channel transport and various numerical methods have been developed to compute the dielectric boundary forces [37–39].

The main objective of this paper is to develop the method of image approximation to the reaction field of the solvent/membrane region surrounding an ion-channel model for the computer simulations of biological ion channels [40–42], which are of interest in many fields such as electrophysiology, cell biology and biomedical science [43, 44]. In order to achieve this goal, we will find image approximations to electric potential in the presence of two types of material interfaces: the layered medium from membranes and a cylindrical region from the ion channel. Then, by combining the results of the image approximations for the two types of interfaces, we will be able to derive the image charge approximation of the reaction field of the ion-channel model. In the hybrid model for the ion-channel simulations, the explicit region is usually chosen as a finite cylindrical geometry, which includes the interested transmembrane proteins, some ions and waters, and a portion of membrane residues. Outside the finite height cylinder, the membrane and bulk solvent are treated implicitly as a continuum medium by the mean field approximation (refer to Fig. 5). Previously, for solvents of pure water, the image method was developed [35] to calculate the reaction field in the ion-channel model. However, the treatment of ionic effects of the electrolyte solution in the ion-channels with the image charge approximation remains unsolved. As the inverse Debye-Hückel screening length in the solvents does not vanish fast enough in many applications, the classical expression of the reaction potential as an infinite sum [45] does not apply directly. In this paper, we will extend our previous results on image approximation to the ion-channel model to the electrolyte solution/membrane environment.

To proceed, we first start with the exact series solution of the reaction potential of a point charge located within a layered dielectric/electrolyte medium because a cell membrane is usually described by a layer embedded in electrolyte solvents. By using this solution, several approximation methods based on least squares are proposed to find the discrete image charges. Then, we derive the image approximation of the reaction field in the presence of infinite cylinder using the method in [35]. Next, combining these two results, we obtain the image approximation of the reaction field for our ion-channel model.

The organization of this paper is as follows. In Sect. 2, the exact solution of a layered system with ionic effects in the solvent layers is discussed. In Sect. 3, the approximate methods of discrete image charges are proposed in layered media. In Sect. 4, the approximate methods are applied to an ion-channel model, and tested by numerical examples. Conclusions are given in Sect. 5.

2 Series Solution for a Layered Medium

Let us start with a classical electric potential problem. Consider a three-layer model representing the dielectric environment of a cell membrane immersed in ionic fluids, as shown in Fig. 1. The cell membrane is treated as an infinite layer (region II), separated from the bulk solvents (region I and III) by two parallel planes. A point charge q_s is located at $\mathbf{x}_s$ inside region II. As the membrane is made of hydrocarbons, it can be described by a dielectric continuum with a low dielectric constant ε_m; typically, $\varepsilon_m = 2$. The electric potential Φ_m in the membrane layer, i.e., in the intermediate layer, satisfies a Poisson equation [46],

$$\Delta \Phi_m(\mathbf{x}, \mathbf{x}_s) = -\frac{4\pi q_s}{\varepsilon_m} \delta(\mathbf{x} - \mathbf{x}_s), \tag{1}$$

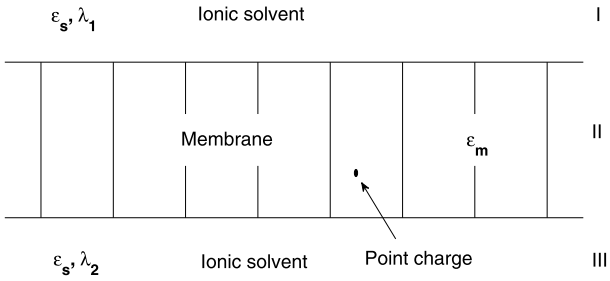

Fig. 1 Schematic illustration of a three-layer model

where $\delta(\cdot)$ is the Dirac delta function.

The ionic solvents in areas I and III are characterized by dielectric permittivities ε_s and parameters of the inverse Debye-Hückel length, λ_1 and λ_2. The potentials in these two regions are governed by the linearized Poisson-Boltzmann equation [2] under the mean field approximation [6],

$$\Delta\Phi - \lambda^2\Phi = 0, \quad \lambda = \sqrt{\frac{8\pi N_A e^2 I}{1000\varepsilon_S k_B T}}, \tag{2}$$

where N_A is Avogadro's number, e is the electron charge, I is the ionic concentration of $1:1$ salt in the bulk solution, k_B is the Boltzmann constant and T is the temperature. We denote the potentials of these two regions by Φ_{up} and Φ_{down}, respectively.

The potential Φ_m inside the membrane layer can be rewritten as a sum of a Coulombic contribution $\Phi_{coul}(\mathbf{x}, \mathbf{x}_s) = q_s/\varepsilon_m|\mathbf{x} - \mathbf{x}_s|$ and a reaction potential Φ_{rf}, due to the polarization of the ionic solvents by the source charge q_s. By expanding both sides of the Poisson equation (1) with orthonormal functions and using the vanishing condition of the Coulombic potential at ∞, the potential Φ_{coul} can be expanded as follows,

$$\frac{q_s}{\varepsilon_m|\mathbf{x} - \mathbf{x}_s|} = \int_0^{+\infty}\int_0^{+\infty} d\alpha d\beta \cos\alpha(x - x_s)\cos\beta(y - y_s)\frac{2q_s}{\varepsilon_m \pi\gamma} e^{-\gamma|z - z_s|}, \tag{3}$$

where $\gamma = \sqrt{\alpha^2 + \beta^2}$. Equation (3) is a Sommerfeld-type identity well known in electromagnetic scattering theory [47, 48].

As Φ_{rf} satisfies the Laplace equation in region II and Φ_{up} and Φ_{down} satisfy the linearized Poisson-Boltzmann equation (2), respectively, these three potentials can also be expanded as,

$$\begin{aligned}\Phi_{rf}(\mathbf{x}, \mathbf{x}_s) = &\int_0^{+\infty}\int_0^{+\infty} d\alpha d\beta \cos\alpha(x - x_s)\cos\beta(y - y_s) \\ &\times [A(\alpha, \beta)e^{\gamma z} + B(\alpha, \beta)e^{-\gamma z}],\end{aligned} \tag{4}$$

$$\Phi_{up}(\mathbf{x}, \mathbf{x}_s) = \int_0^{+\infty}\int_0^{+\infty} d\alpha d\beta \cos\alpha(x - x_s)\cos\beta(y - y_s)C(\alpha, \beta)e^{-\sqrt{\gamma^2 + \lambda_1^2}z}, \tag{5}$$

$$\Phi_{down}(\mathbf{x}, \mathbf{x}_s) = \int_0^{+\infty}\int_0^{+\infty} d\alpha d\beta \cos\alpha(x - x_s)\cos\beta(y - y_s)D(\alpha, \beta)e^{\sqrt{\gamma^2 + \lambda_2^2}z}. \tag{6}$$

Suppose the planar surfaces are located at $z = 0$ and $z = l$ with l being the thickness of the membrane. Two interface conditions for the continuities of the potential and the normal

displacement at each interface are given by,

$$\Phi_m = \Phi_{down}, \quad \varepsilon_m \frac{\partial \Phi_m}{\partial z} = \varepsilon_s \frac{\partial \Phi_{down}}{\partial z}, \quad \text{for } z = 0, \tag{7}$$

$$\Phi_m = \Phi_{up}, \quad \varepsilon_m \frac{\partial \Phi_m}{\partial z} = \varepsilon_s \frac{\partial \Phi_{up}}{\partial z}, \quad \text{for } z = l. \tag{8}$$

Substituting the boundary conditions (7) and (8) into expressions (3)–(6) yields a linear system for the coefficients A, B, C and D,

$$\begin{cases} \frac{2q}{\varepsilon_m \pi \gamma} e^{-\gamma z_s} + A + B = D, \\ \frac{2q}{\varepsilon_m \pi} e^{-\gamma z_s} + \gamma A - \gamma B = \frac{\varepsilon_s}{\varepsilon_m} \sqrt{\gamma^2 + \lambda_2^2} D, \\ \frac{2q}{\varepsilon_m \pi \gamma} e^{-\gamma (l - z_s)} + A e^{\gamma l} + B e^{-\gamma l} = C e^{-\sqrt{\gamma^2 + \lambda_1^2} l}, \\ -\frac{2q}{\varepsilon_m \pi} e^{-\gamma (l - z_s)} + \gamma A e^{\gamma l} - \gamma B e^{-\gamma l} = -\frac{\varepsilon_s}{\varepsilon_m} \sqrt{\gamma^2 + \lambda_1^2} C e^{-\sqrt{\gamma^2 + \lambda_1^2} l}. \end{cases} \tag{9}$$

For convenience, let $\varepsilon = \frac{\varepsilon_s}{\varepsilon_m}$, $\tau_i = \varepsilon \sqrt{\gamma^2 + \lambda_i^2}$, $i = 1, 2$. Solving the linear system (9) leads to the coefficients in the reaction potential Φ_{rf} (4),

$$A(\alpha, \beta) = \frac{2q_s}{\varepsilon_m \pi \gamma} \frac{e^{-\gamma (l - z_s)} (\gamma - \tau_1)(\gamma + \tau_2) + e^{-\gamma (l + z_s)} (\gamma - \tau_1)(\gamma - \tau_2)}{(\gamma + \tau_1)(\gamma + \tau_2) e^{\gamma l} - (\gamma - \tau_1)(\gamma - \tau_2) e^{-\gamma l}}, \tag{10}$$

$$B(\alpha, \beta) = \frac{2q_s}{\varepsilon_m \pi \gamma} \frac{e^{\gamma (l - z_s)} (\gamma + \tau_1)(\gamma - \tau_2) + e^{-\gamma (l - z_s)} (\gamma - \tau_1)(\gamma - \tau_2)}{(\gamma + \tau_1)(\gamma + \tau_2) e^{\gamma l} - (\gamma - \tau_1)(\gamma - \tau_2) e^{-\gamma l}}. \tag{11}$$

Series solutions for the reaction field in layered media of more than three layers can be found in Appendix.

3 Method of Image Charges in Layered Inhomogeneities

In this section, we will study the use of the image charge representation and approximation to the reaction field in layered inhomogeneous dielectrics/solutions.

3.1 A Layered and Non-ionic Solution—RIC Method

First, let us consider the case of pure water where no free charge is presented in the solvents (pure water), then, the inverse Debye-Hückel length $\lambda_1 = \lambda_2 = 0$. For this case, a rectangular image charge (RIC) method was used for the reaction field [45], where the reaction potential for a point charge in a rectangular infinite system was suggested as,

$$\Phi_{rf}(\mathbf{x}, \mathbf{x}_s) = \sum_{k=-\infty,\ k \neq 0}^{k=+\infty} \frac{Q_k}{\varepsilon_m |\mathbf{x} - \mathbf{x}_k|}, \tag{12}$$

with

$$\mathbf{x}_k = \left(x_s, y_s, (-1)^k \left(z_s - \frac{l}{2} \right) + \left(k + \frac{1}{2} \right) l \right), \qquad Q_k = q_s \left(\frac{\varepsilon_m - \varepsilon_s}{\varepsilon_m + \varepsilon_s} \right)^{|k|}.$$

Here, we will illustrate the mathematical equivalence between the expression (4) and (12) when $\lambda_1 = \lambda_2 = 0$. Recall that $\tau_1 = \tau_2 = \varepsilon\gamma$ in this case, then expression (4) can be rewritten into four parts as

$$\Phi_{rf}(\mathbf{x}, \mathbf{x}_s) = \int_0^{+\infty}\int_0^{+\infty} d\alpha d\beta \cos\alpha(x - x_s)\cos\beta(y - y_s)[I + II + III + IV]$$

$$I = \frac{2q}{\varepsilon_m \pi\gamma}\frac{e^{-\gamma(2l - z_s - z)}(\frac{1-\varepsilon}{1+\varepsilon})}{1 - e^{-2\gamma l}(\frac{1-\varepsilon}{1+\varepsilon})^2}, \qquad II = \frac{2q}{\varepsilon_m \pi\gamma}\frac{e^{-\gamma(2l + z_s - z)}(\frac{1-\varepsilon}{1+\varepsilon})^2}{1 - e^{-2\gamma l}(\frac{1-\varepsilon}{1+\varepsilon})^2},$$

$$III = \frac{2q}{\varepsilon_m \pi\gamma}\frac{e^{\gamma(-z_s - z)}(\frac{1-\varepsilon}{1+\varepsilon})}{1 - e^{-2\gamma l}(\frac{1-\varepsilon}{1+\varepsilon})^2}, \qquad IV = \frac{2q}{\varepsilon_m \pi\gamma}\frac{e^{-\gamma(2l - z_s + z)}(\frac{1-\varepsilon}{1+\varepsilon})^2}{1 - e^{-2\gamma l}(\frac{1-\varepsilon}{1+\varepsilon})^2}. \tag{13}$$

As $|e^{-2\gamma l}(\frac{1-\varepsilon}{1+\varepsilon})^2| < 1$, the denominator in (13) can be expanded as a geometric progression,

$$\frac{1}{1 - e^{-2\gamma l}(\frac{1-\varepsilon}{1+\varepsilon})^2} = \sum_{k=0}^{k=+\infty} e^{-2k\gamma l}\left(\frac{1-\varepsilon}{1+\varepsilon}\right)^{2k} = \sum_{k=0}^{k=-\infty} e^{2k\gamma l}\left(\frac{1-\varepsilon}{1+\varepsilon}\right)^{-2k},$$

then, (13) becomes:

$$\begin{aligned}
\Phi_{rf}(\mathbf{x}, \mathbf{x}_s) = &\sum_{k=0}^{k=+\infty}\int_0^{+\infty}\int_0^{+\infty} d\alpha d\beta \cos\alpha(x - x_s)\cos\beta(y - y_s)\frac{2q}{\varepsilon_m \pi\gamma} \\
&\times\left(e^{-\gamma(2kl + 2l - z_s - z)}\left(\frac{1-\varepsilon}{1+\varepsilon}\right)^{2k+1} + e^{-\gamma(2kl + 2l + z_s - z)}\left(\frac{1-\varepsilon}{1+\varepsilon}\right)^{2k+2}\right) \\
&+ \sum_{k=0}^{k=-\infty}\int_0^{+\infty}\int_0^{+\infty} d\alpha d\beta \cos\alpha(x - x_s)\cos\beta(y - y_s)\frac{2q}{\varepsilon_m \pi\gamma} \\
&\times\left(e^{\gamma(2kl - z_s - z)}\left(\frac{1-\varepsilon}{1+\varepsilon}\right)^{-2k+1} + e^{-\gamma(-2kl + 2l - z_s + z)}\left(\frac{1-\varepsilon}{1+\varepsilon}\right)^{-2k+2}\right) \\
= &\sum_{k=0}^{k=+\infty}\frac{Q_{2k+1}}{\varepsilon_m|\mathbf{x} - \mathbf{x}_{2k+1}|} + \frac{Q_{2k+2}}{\varepsilon_m|\mathbf{x} - \mathbf{x}_{2k+2}|} + \sum_{k=0}^{k=-\infty}\frac{Q_{2k-1}}{\varepsilon_m|\mathbf{x} - \mathbf{x}_{2k-1}|} + \frac{Q_{2k-2}}{\varepsilon_m|\mathbf{x} - \mathbf{x}_{2k-2}|} \\
= &\sum_{k=-\infty,\ k\neq 0}^{k=+\infty}\frac{Q_k}{\varepsilon_m|\mathbf{x} - \mathbf{x}_k|},
\end{aligned}$$

where the second last equation holds from the Sommerfeld identity (3). Hence, the proof for the equivalence between the expression (4) and (12).

It should also be mentioned that image formula (12) in fact approximates the solution to the ionic case (2) with an accuracy of $O(\lambda)$ and the proof is technical, but straightforward and omitted here.

3.2 Layered Ionic Solutions

In this case, although the integrand in expression (4) of Φ_{rf} is damped exponentially at high frequencies, numerical integration of Φ_{rf} is still time consuming. In simulations of

biological systems, image charge methods [25, 26] are widely used to speed up the calculation of electrostatic interactions. In particular, the method of multiple images [30] was developed to treat the electrostatic reaction field of spherical geometries with high accuracy, which is based on a numerical quadrature of line image representation [49–51]. The key of multiple image methods is to find some image points such that their electrostatic potentials give an accurate approximation to the sought-after reaction field,

$$\Phi_{irf}(\mathbf{x}, \mathbf{x}_s) = \frac{q_s}{\varepsilon_m} \sum_k \frac{q_k}{|\mathbf{x} - \mathbf{x}_k|}, \tag{14}$$

where unknown q_k and $\mathbf{x}_k$ are the strength and the location of the kth image charge with a dependence on the location $\mathbf{x}_s$ of the unit source charge. The technique used in proving the RIC method is not applicable here as the integral becomes too complicated. Here, we introduce two ways to obtain the image charge approximation and present corresponding numerical test results.

In the first method, the locations of the image charges are pre-fixed at the locations given in the RIC method (12) and their magnitudes are obtained through a least square procedure. In the second method, both the locations and the magnitudes of the image charges are produced through a Prony type approximation to the Fourier transform of the reaction potential and the Sommerfeld type identity (3).

3.2.1 Method Based on Least Square Fitting the Reaction Potential with Image-Based Potentials

Set N monitoring points inside the membrane layer denoted as $\hat{\mathbf{x}}_n, n = 1, 2, \ldots, N$, and consider the image charges in pairs, i.e., the kth pair of image charges locate at $\mathbf{x}_{\pm k}$. In order to be consistent with the RIC method, we fix $\mathbf{x}_{\pm k}$ as

$$\mathbf{x}_k = \left(x_s, y_s, (-1)^k \left(z_s - \frac{l}{2}\right) + \left(k + \frac{1}{2}\right) l\right), \quad k = \pm 1, \pm 2, \ldots.$$

Then, the L_2 error between the image-based potential field and the exact reaction field reads:

$$Err(\{q_{\pm k}\}|_{k=1}^K) = \sqrt{\frac{\sum_{n=1}^N [\Phi_{irf}(\hat{\mathbf{x}}_n, \mathbf{x}_s) - \Phi_{rf}(\hat{\mathbf{x}}_n, \mathbf{x}_s)]^2}{\sum_{n=1}^N \Phi_{rf}(\hat{\mathbf{x}}_n, \mathbf{x}_s)^2}}. \tag{15}$$

Solving the minimization problem yields the value of $q_{\pm k}$. In fact, the error function is a quadratic function of $q_{\pm k}$, so the minimization problem is easy to solve.

A simple Mathematica code is developed to calculate the strength of image charges for each set of dielectric parameters and Debye length, the "FindMinimum" subroutine is used to solve the minimization problem. To show the performance of the code, we set $\varepsilon_m = 1$, $\varepsilon_s = 80$, $\lambda_1 = 2.5$ and $\lambda_2 = 0.5$, here the $\varepsilon_s = 80$ represents the water dielectric, and a relative small ε_m represents a dielectric constant of membrane lipids. As the origin of x-y plane should not influence the calculation, we set the source charges at $(0, 0, z_s)$ without loss of the generality. In all calculations, we take $N = 512$ monitoring points uniformly distributed in a rectangle centered at $(0, 0, 0.5l)$, here l, the thickness of membrane, is set to be $l = 1$ as a dimensionless parameter.

We set $K = 2$, i.e., four image charges are used to approximate the reaction field. Numerical tests show that this choice gives satisfactory accuracy. The locations of these four

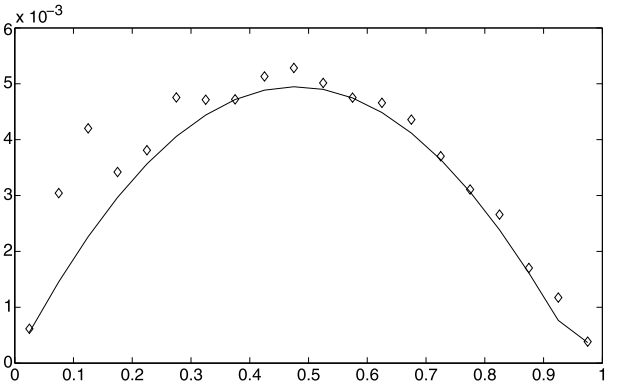

Fig. 2 Relative errors (15) of the reaction field with four images, the diamonds: images given by the (16), and the solid line: images obtained by least square minimization (15)

image charges are

$$\mathbf{x}_{-2} = (0, 0, -2l + z_s), \qquad \mathbf{x}_{-1} = (0, 0, -z_s),$$
$$\mathbf{x}_1 = (0, 0, 2l - z_s), \qquad \mathbf{x}_2 = (0, 0, 2l + z_s).$$

To find the systematic dependence of the image charges on the location of the source charge z_s, we fit the numerical results of $q_{\pm 1}, q_{\pm 2}$ at selected choices of z_s by an analytical function of $\hat{z}_s = z_s/l$. Sixth order polynomials plus a term $1/\hat{z}_s$ are used for this purpose. The resulting image charges for a range of the fitted source location z_s gives approximation to the reaction field at the corresponding source charge within an error less than 1%. The exact dependence on z_s is summarized in the following relation.

By denoting,

$$\overrightarrow{q} = (q_{-2}, q_{-1}, q_1, q_2)^{\mathrm{T}}, \qquad \overrightarrow{Z}_s = (\hat{z}_s^6, \hat{z}_s^5, \hat{z}_s^4, \hat{z}_s^3, \hat{z}_s^2, \hat{z}_s, 1, 1/\hat{z}_s)^{\mathrm{T}},$$

we have

$$\overrightarrow{q} = C_1 \overrightarrow{Z}_s, \tag{16}$$

where

$$C_1 = \begin{pmatrix} 58.3268 & -167.32 & 187.036 & -102.557 & 28.073 & -2.7127 & 0.2281 & -0.0035 \\ -58.4118 & 167.471 & -187.089 & 102.925 & -28.772 & 4.0046 & -1.1982 & 0.0035 \\ -0.1335 & 0.4557 & -0.6430 & 0.3289 & 0.3440 & -0.6359 & -0.7012 & 0.0014 \\ 0.2214 & -0.6194 & 0.7137 & -0.6954 & -0.0167 & -0.3011 & 0.6732 & -0.0014 \end{pmatrix}.$$

Figure 2 shows both the relative error (15) by computing the reaction field by using image charges obtained directly from solving the minimization problem (15) and those given by the fitting function (16). The small difference indicates that we can use image charges given by (16) for computing the reaction field for any z_s in the fitted range.

3.2.2 Method Based on a Prony Fitting of the Fourier Transform of the Reaction Potential

The second method to construct the image charges is based on a Prony approximation [52, 53], where a sum of exponentials is used to approximate the Fourier transform of the

exact reaction field potential. Rewrite the exact reaction field (4) in the following form,

$$\Phi_{rf}(\mathbf{x},\mathbf{x}_s)=\int_0^{+\infty}\int_0^{+\infty} d\alpha d\beta\ \cos\alpha(x-x_s)\cos\beta(y-y_s)\frac{2q_s}{\varepsilon_m\pi\gamma}[\hat{A}e^{\gamma z}+\hat{B}e^{-\gamma z}], \quad (17)$$

where

$$\begin{aligned}\hat{A}(\gamma)&=\frac{e^{-\gamma(l-z_s)}(\gamma-\tau_1)(\gamma+\tau_2)+e^{-\gamma(l+z_s)}(\gamma-\tau_1)(\gamma-\tau_2)}{(\gamma+\tau_1)(\gamma+\tau_2)e^{\gamma l}-(\gamma-\tau_1)(\gamma-\tau_2)e^{-\gamma l}},\\ \hat{B}(\gamma)&=\frac{e^{\gamma(l-z_s)}(\gamma+\tau_1)(\gamma-\tau_2)+e^{-\gamma(l-z_s)}(\gamma-\tau_1)(\gamma-\tau_2)}{(\gamma+\tau_1)(\gamma+\tau_2)e^{\gamma l}-(\gamma-\tau_1)(\gamma-\tau_2)e^{-\gamma l}}.\end{aligned} \quad (18)$$

Comparing this expression with the Sommerfeld identity (3), and using the symmetry of the rectangular system, a natural approach is to approximate the function $\hat{A}(\gamma)$ and $\hat{B}(\gamma)$ by a sum of exponential functions as,

$$\begin{aligned}\hat{A}^{app}(\gamma)&=\sum_{k=1}^{K}\left(a_{2k-1}e^{-(z_{2k-1}-c_k)\gamma}+a_{2k}e^{-(z_{2k}+c_k)\gamma}\right),\\ \hat{B}^{app}(\gamma)&=\sum_{k=-1}^{-K}\left(a_{2k+1}e^{(z_{2k+1}+c_k)\gamma}+a_{2k}e^{(z_{2k}-c_k)\gamma}\right),\end{aligned}$$

where $z_k=(-1)^k(z_s-\frac{l}{2})+(k+\frac{1}{2})l$ are the location of image charges in the case $\lambda_1=\lambda_2=0$, $a_{\pm k}, c_{\pm k}$ are unknown variations of the kth pair image charges. Imposing the following conditions:

$$\begin{aligned}&z_{2k-1}-c_k>l, \quad z_{2k}+c_k>l, \quad \text{for } k>0,\\ &z_{2k+1}+c_k<0, \quad z_{2k}-c_k<0, \quad \text{for } k<0,\end{aligned}$$

then applying the Sommerfeld type identity (3) yields:

$$\begin{aligned}\Phi_{irf}(\mathbf{x},\mathbf{x}_s)=&\int_0^{+\infty}\int_0^{+\infty} d\alpha d\beta\cos\alpha(x-x_s)\cos\beta(y-y_s)\frac{2q_s}{\varepsilon_m\pi\gamma}\\ &\times\left[\sum_{k=1}^{K}(a_{2k-1}e^{-(z_{2k-1}-c_k-z)\gamma}+a_{2k}e^{-(z_{2k}+c_k-z)\gamma})\right.\\ &\left.+\sum_{k=-1}^{-K}(a_{2k+1}e^{-(z-z_{2k+1}-c_k)\gamma}+a_{2k}e^{-(z-z_{2k}+c_k)\gamma})\right]\\ =&\sum_{k=1}^{K}\frac{q_s}{\varepsilon_m}\left[\frac{a_{2k-1}}{\mathbf{x}-\mathbf{x}_{2k-1}}+\frac{a_{2k}}{\mathbf{x}-\mathbf{x}_{2k}}\right]+\sum_{k=-1}^{-K}\frac{q_s}{\varepsilon_m}\left[\frac{a_{2k+1}}{\mathbf{x}-\mathbf{x}_{2k+1}}+\frac{a_{2k}}{\mathbf{x}-\mathbf{x}_{2k}}\right],\end{aligned} \quad (19)$$

with

$$\mathbf{x}_{2k-1}=(x_s,y_s,z_{2k-1}-c_k), \quad \mathbf{x}_{2k}=(x_s,y_s,z_{2k}+c_k), \quad k>0, \quad (20)$$

$$\mathbf{x}_{2k+1}=(x_s,y_s,z_{2k+1}+c_k), \quad \mathbf{x}_{2k}=(x_s,y_s,z_{2k}-c_k), \quad k<0. \quad (21)$$

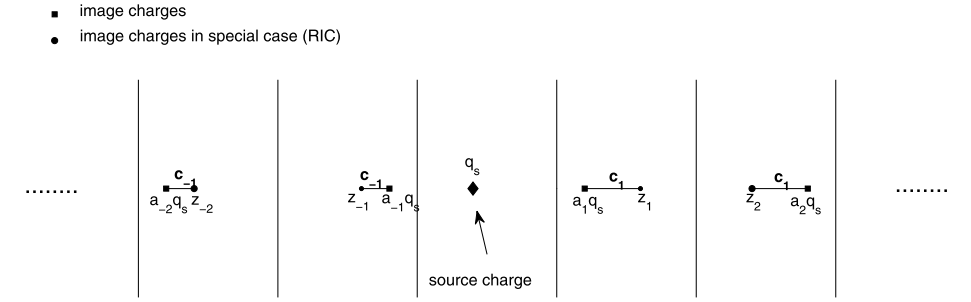

Fig. 3 The physical meaning of a_k and c_k, taking $k = \pm 1$ for example

Table 1 Convergence of J-sampling Fourier transform of reaction potential

J	4	6	8	10
$\max_{z_s \in (0,l)} \sqrt{\sum_{t=1}^{100} \frac{(\hat{A}(\frac{t}{10}) - \hat{A}^{app}(\frac{t}{10}))^2}{100}}$	0.00538	0.00196	0.00080	0.00068
$\max_{z_s \in (0,l)} \sqrt{\sum_{t=1}^{100} \frac{(\hat{B}(\frac{t}{10}) - \hat{B}^{app}(\frac{t}{10}))^2}{100}}$	0.00928	0.00571	0.00658	0.00630

Once a_k and c_k are found, the image charges are given by the Sommerfeld type identity (3), Fig. 3 shows the geometric meaning of a_k and c_k. As functions $\hat{A}(\gamma)$ and $\hat{B}(\gamma)$ are smoothly damped exponentials, such an approximation is reasonable and effective. The parameter a_k and c_k can be calculated by solving a simple minimization problem of the L_2 errors, sampling γ at γ_j, $j = 1, 2, \ldots, J$. The L_2 error of the approximate function and the exact function can be written as,

$$Err_A(\{a_{2k-1}, a_{2k}, c_k\}|_{k=1}^{K}) = \sqrt{\sum_{j=1}^{J} (\hat{A}(\gamma_j) - \hat{A}^{app}(\gamma_j))^2 / J}, \tag{22}$$

and

$$Err_B(\{a_{2k+1}, a_{2k}, c_k\}|_{k=-1}^{-K}) = \sqrt{\sum_{j=1}^{J} (\hat{B}(\gamma_j) - \hat{B}^{app}(\gamma_j))^2 / J}. \tag{23}$$

We use the same parameters as the previous method: $\varepsilon_m = 1, \varepsilon_s = 80, \lambda_1 = 2.5, \lambda_2 = 0.5$ and $l = 1$. The source charge is supposed to locate at $(0, 0, z_s)$. Choosing $K = 1$, i.e., two exponentials to approximate each of $\hat{A}$ and $\hat{B}$. Here let γ_j be the scaled Chebyshev interpolation points in the interval $[0, 10]$. For the choice of J, the number of sampling points, the Table 1 shows the decay of L_2 errors in terms of increasing J.

The numerical tests show $J = 10$ is a good enough choice with an overall error less than 0.1%. Again as before, by least squares fitting the data at selected z_s, we can obtain an analytical dependence of the coefficients on z_s as follows.

Setting $\hat{z}_s = z_s / l$ and

$$\overrightarrow{a} = (a_1, a_2, a_{-1}, a_{-2}, c_1, c_{-1})^{\mathrm{T}}, \qquad \overrightarrow{Z}_s = (\hat{z}_s^6, \hat{z}_s^5, \hat{z}_s^4, \hat{z}_s^3, \hat{z}_s^2, \hat{z}_s, 1)^{\mathrm{T}}$$

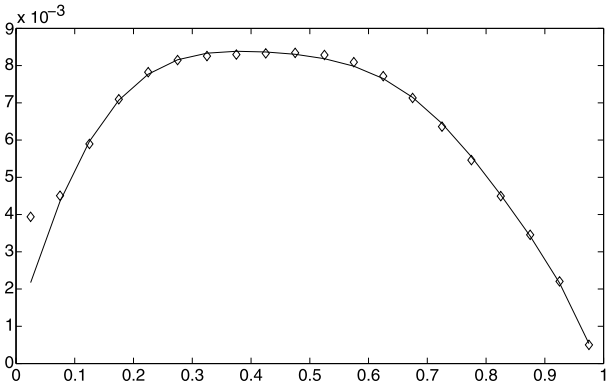

Fig. 4 Relative errors of the reaction field with four images, the diamonds: images given by (24) and (20)–(21), and the solid line: images obtained by minimizing (22)–(23) and (20)–(21)

we have

$$\overrightarrow{a} = C_2 \overrightarrow{Z}_s, \tag{24}$$

where

$$C_2 = \begin{pmatrix} -0.7897 & 3.1309 & -4.9024 & 3.5424 & -0.4660 & -1.4715 & -0.0384 \\ 0.7888 & -3.1316 & 4.9043 & -3.5493 & 0.46723 & 0.5071 & 0.0130 \\ -3.5602 & 9.7702 & -9.5473 & 4.6495 & -0.5400 & 0.1877 & -0.9766 \\ 3.6741 & -10.101 & 9.8343 & -4.6115 & 0.3358 & 0.8773 & 0.0030 \\ -5.7251 & 20.3875 & -28.9648 & 20.7972 & -7.5971 & 0.7714 & 0.3235 \\ -4.6749 & 12.8514 & -13.3379 & 6.6873 & -1.3877 & 0.1440 & -0.0029 \end{pmatrix}.$$

Analogously, the L_2 error function between the image-based potential and the exact reaction field reads,

$$Err(\{a_{\pm(2k-1)}, a_{\pm 2k}, c_{\pm k}\}|_{k=1}^{K}) = \sqrt{\frac{\sum_{n=1}^{N}[\Phi_{irf}(\hat{\mathbf{x}}_n, \mathbf{x}_s) - \Phi_{rf}(\hat{\mathbf{x}}_n, \mathbf{x}_s)]^2}{\sum_{n=1}^{N} \Phi_{rf}(\hat{\mathbf{x}}_n, \mathbf{x}_s)^2}}. \tag{25}$$

Figure 4 shows both the relative error (25) by computing the reaction field by using image charges obtained directly from solving the minimization problem (22)–(23) and those given by the fitting function (24). The small difference indicates that we can use image charges given by (24) ((20)–(21)) for computing the reaction field for any z_s in the fitted range. The numerical test shows that both two approximate methods provide satisfactory accuracy, while the second one is much simpler as the user only needs to deal with the integrand. The fitting functions in both methods only depend on the dielectric permittivities ε_m, ε_s and Debye length λ_1, λ_2. The Mathematica program is available (upon request to the author) for generating such functions.

4 Method of Image Charges in an Ion-Channel Model

In this section, we will construct image charge approximation to the reaction field in an ion-channel model as Fig. 5, which includes three dielectric areas: a finite cylinder, the membrane surrounding the cylinder, and the bulk solvents (upper and lower semi-infinite layers), these three areas are characterized by dielectric constants ε_0, ε_m and ε_s, respectively. Such

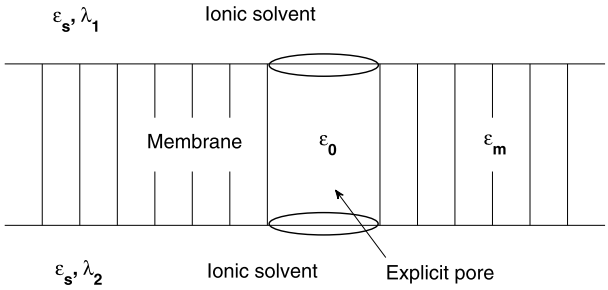

Fig. 5 Schematic illustration of an ion channel model

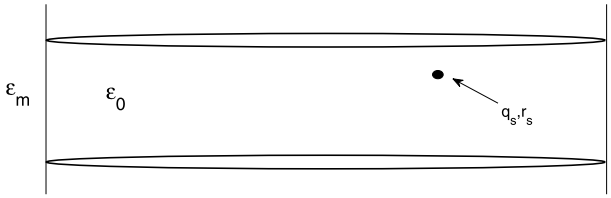

Fig. 6 Schematic illustration of an infinite cylinder

a model involves inhomogeneity of layered and cylindrical structures. We will handle each type individually, and then combine the results to address the ion-channel inhomogeneity.

First, for the infinite cylinder system, see Fig. 6, consider a point charge q_s located at position $\mathbf{r}_s$ inside the cylinder, denote the radius of the cylinder as a, the cylinder partitions the whole space into two regions, characterized by ε_0 and ε_m.

According to [35], the reaction potential of point charge $(q_s, \mathbf{r}_s)$ can be approximated as

$$\Phi_{rf}^{cylinder}(\mathbf{r}, \mathbf{r}_s) = \frac{q_s}{\varepsilon_0} \sum_{c=1}^{C} \frac{f_c}{|\mathbf{r} - \mathbf{x}_c|}. \tag{26}$$

Suppose $\mathbf{r}_s = (\rho_s, \varphi_s, z_s)$ under the cylindrical coordinate system. Here $\mathbf{x}_c = (\rho_c, \varphi_s + \varphi_c, z_s)$, f_c, ρ_c, φ_c can be generated by a function depending on ε_0 and ε_m. Especially, if $\varepsilon_0 = 1$, $\varepsilon_m = 2$, and $C = 3$, the three image charges are $(f_c, \rho_c, \varphi_c) = \{(f_1, \rho_1, 0), (f_2, \rho_2, \pm\varphi_2)\}$. Let $p = \rho_s/a$, we have the following dependence of the image charges on the location of the source charge ρ_s [35].

Setting

$$\overrightarrow{f} = (f_1, \rho_1/a, f_2, \rho_2/a, \varphi_2)^{\mathrm{T}}, \qquad \overrightarrow{p} = (p^5, p^4, p^3, p^2, p, 1)^{\mathrm{T}}$$

we have

$$\overrightarrow{f} = C_3 \overrightarrow{p}, \tag{27}$$

where

$$C_3 = \begin{pmatrix} 0.6017 & -0.3404 & -0.3575 & 0.1087 & -0.1786 & -0.2056 \\ 0.1325 & -0.9731 & 0.9896 & -0.4172 & -0.2402 & 1.5140 \\ -0.5329 & 0.6471 & -0.1531 & 0.0826 & 0.0790 & -0.2065 \\ 5.0993 & -8.5071 & 5.0090 & -1.5284 & 0.2496 & 1.5133 \\ -10.4528 & 21.7663 & -14.4548 & 4.1924 & -1.3155 & 2.1019 \end{pmatrix}.$$

Now we will combine this result with the results of layered media in previous section to address the inhomogeneity of the ion-channel model in Fig. 5.

Let us assume that the source charge q_s is at $\mathbf{r}_s = \mathbf{x}_0 = (\rho_0, \varphi_s + \varphi_0, z_s)$ inside an infinite cylinder with a radius of the ion channel size a. The dielectric constant inside the cylinder is that of the cavity (close to 1–2) and the dielectric constant outside the cylinder is taken as that of the membrane. The cylindrical interface will require the following image charges $f_c q_s$, $c = 1, \ldots, C$ for the approximation of the reaction field potential as in (26). Now, we introduce the planar membrane/solvent interfaces at $z = 0, l$, which will generate $2K$ image charges $q_s q_k$ and $f_c q_s q_k$, $k = \pm 1, \ldots, \pm K$ for the approximation of the reaction field as in (14) for each of the charges q_s and $f_c q_s$. Altogether, the reaction field for the ion-channel model can now be approximated by the potential of $(2K + 1)(C + 1) - 1$ image charges as

$$\Phi_{rf}(\mathbf{r}, \mathbf{r}_s) \approx \frac{q_s}{\varepsilon_o} \sum_{c=0}^{C} \sum_{k=-K}^{K} \frac{(1 - \delta_{c0}\delta_{k0}) f_c q_k}{|\mathbf{r} - \mathbf{x}_{c,k}|}, \tag{28}$$

where $\mathbf{x}_{c,k}$ is the image charge point given in (14) indexed by k in rectangular infinite system for the source charge located at $\mathbf{x}_c$.

Remark 1 Notice that (28) is obtained under the assumption the medium between the planes is homogeneous, which implies that we have to ignore the difference in the dielectric constants of the membrane and the interior of the cylinder (chosen close to the vacuum). This is justified as in this case both of them are small compared to the dielectric constant of the solvents (∼80). And the accuracy of the approximation remains acceptable when ε_m reaches as large as 20, which will be shown below.

The accuracy of the image solution (28) is tested by calculating the self energy $V(\mathbf{r}_s) = q_s \Phi_{rf}(\mathbf{r}_s)/2$ of a unit point charge located within the finite cylinder. The radius and the height of the cylinder is 4 Å and 12 Å. At first, we set the source charge at $(x, 0, z)$, where x takes two values, 0 and 2 Å, and z varies from 3 to 9 Å. For a reference solution, the Poisson-Boltzmann equation is solved by the following 3D finite difference method in [54] for the ion-channel model with uniform grids of size $h = 0.5$ Å.

$$\begin{aligned}
&\varepsilon_x(i, j, k)[\Phi(i + 1, j, k) - \Phi(i, j, k)] + \varepsilon_x(i - 1, j, k)[\Phi(i - 1, j, k) - \Phi(i, j, k)] \\
&\quad + \varepsilon_y(i, j, k)[\Phi(i, j + 1, k) - \Phi(i, j, k)] + \varepsilon_y(i, j - 1, k)[\Phi(i, j - 1, k) - \Phi(i, j, k)] \\
&\quad + \varepsilon_z(i, j, k)[\Phi(i, j, k + 1) - \Phi(i, j, k)] + \varepsilon_z(i, j, k - 1)[\Phi(i, j, k - 1) - \Phi(i, j, k)] \\
&\quad - \kappa^2(i, j, k)\Phi(i, j, k)h^2 = -4\pi \frac{q(i, j, k)}{h},
\end{aligned} \tag{29}$$

where $\kappa(i, j, k)$ is the inverse Debye screening length, $q(i, j, k)$ is the fractional charge at the grid point (x_i, y_j, z_k), and $\varepsilon_x(i, j, k)$, $\varepsilon_y(i, j, k)$ and $\varepsilon_z(i, j, k)$ represent the dielectric constants associated with x-, y-, and z-directions at grid branches $(x_i + h/2, y_j, z_k)$, $(x_i, y_j + h/2, z_k)$, and $(x_i, y_j, z_k + h/2)$. The linear algebra problem is solved by the bi-conjugate gradient method with an error tolerance 10^{-8}.

Let $\varepsilon_0 = 1$, $\varepsilon_m = 2$, $\varepsilon_s = 80$, $\lambda_1 = 2.5$ and $\lambda_2 = 0.5$ in the ion-channel model, so that the expression (16), (24) and (27) can be applied directly. Figures 7 and 8 give the comparative result on self energies between the image-based (28) and finite difference method. As 4 images are used to treat the planner interface inhomogeneity and 3 images are used for the cylindrical interface inhomogeneity, this results in a 19 images being used in the image approximation to the reaction field (28) for the ion-channel model. In Figs. 7 and 8, methods

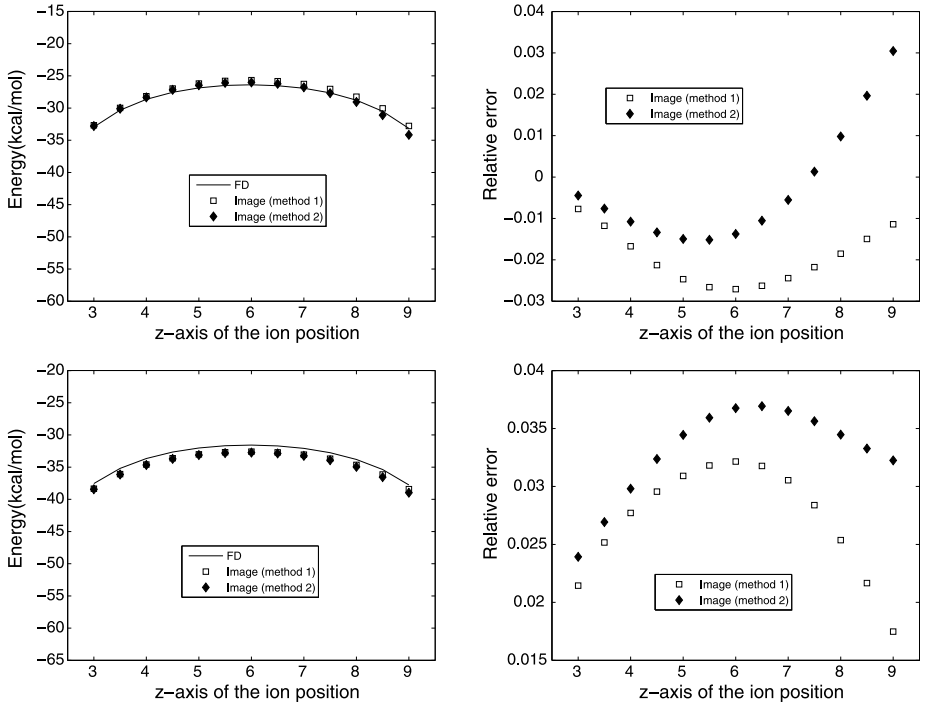

Fig. 7 Self energy of a unit charge located at $(0, 0, z)$ (*top*) and $(2, 0, z)$ (*bottom*) within the channel

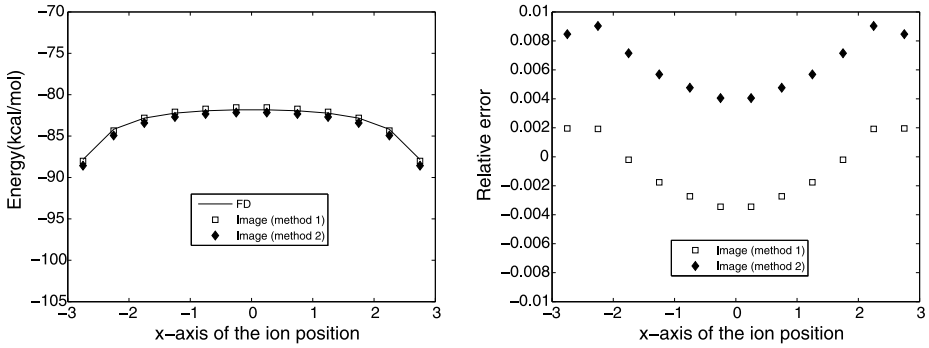

Fig. 8 Self energy of a unit charge located at $(x, 0, 1)$ within the channel

1 and 2 represent the image methods by the least square fitting and the Prony fitting, respectively. In Fig. 7, the relative errors are less than 3% for method 1 and 4% for method 2, and in Fig. 8, the maximum error is about 4%. Figure 8 plots the result for the charge located at $(x, 0, 1)$ (close to the interface between the cylinder and the bottom plane), which shows that the image charge method is accurate even for charges close to the boundary.

Finally, to estimate the accuracy dependence on the dielectric constant of the membrane for the proposed image method, we also calculate the results of the dielectric constant $\varepsilon_m = 20$ by setting all the other parameters the same as above. The error profiles of self

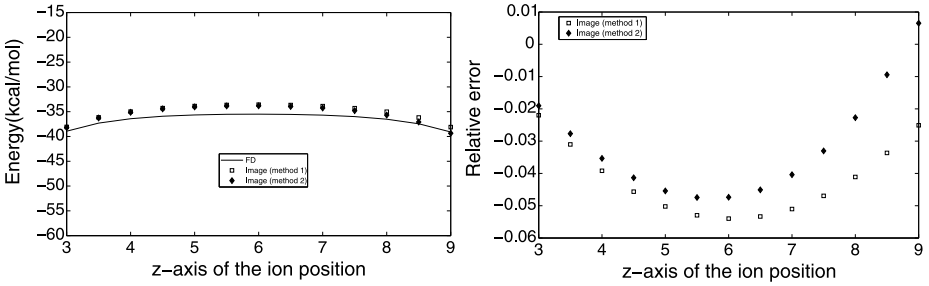

Fig. 9 Self energy of a unit charge located at $(0, 0, z)$ within the channel

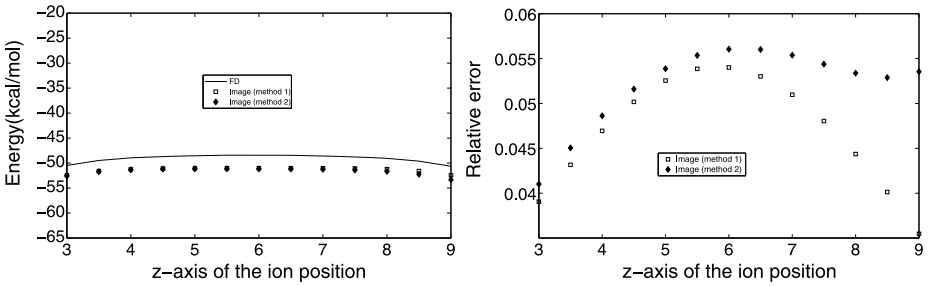

Fig. 10 Self energy of a unit charge located at $(2, 0, z)$ within the channel

energy are shown in Figs. 9 and 10. The image approximation is obtained by an assumption of homogeneity of the region between the two planar interfaces. We can see that although the dielectric jump increases from 1 : 2 to 1 : 20, the accuracy of self energy calculations remains acceptable, for which the maximum error slightly increases from between 3–4% to between 5–6%.

5 Concluding Remarks

Image approximations to the electrical potential in the Poisson-Boltzmann theory for electrolyte solutions and dielectrics in inhomogeneous media such as layered or cylindrical structure are obtained and found to be an accurate and efficient numerical method. Furthermore, the image approximation for the ion-channel configuration will allow the application of hybrid solvation model with a reaction field based molecular dynamics simulation [21] for the selectivity of various ion-channels. The image approximation to the reaction field removed the inhomogeneity of the system such that all electrostatic interactions in the ion-channel and ionic solvent/membrane environment are expressed in terms of Coulombic pairwise interactions among source charges and their image charges. As a result, fast algorithms such as the fast multipole method can be used to model electrostatic interaction in these inhomogeneous media.

Acknowledgements W. Cai acknowledges the financial support from the US Department of Energy (grant number: DEFG0205ER25678) and a NSF grant (grant number DMS-1005441). Z. Xu acknowledges the support from NSFC (grant number: 11026057) and the Chinese Ministry of Education (grant number NCET-09-0556). H. Tang acknowledges the support of NSFC (grant number: 10925101). W. Cai and H. Tang also acknowledge the support of NSFC (grant number: 10828101).

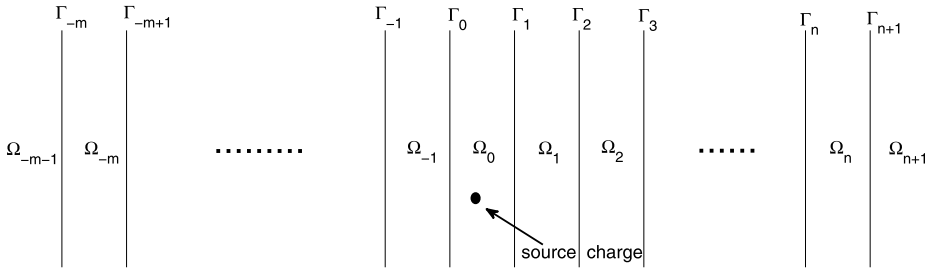

Fig. 11 Schematic illustration of an multi-layered model

Appendix: Series Expansion for a General Multi-Layered System

For a general multi-layered model, which is schematically shown in Fig. 11, the system is divided into several rectangular infinite regions, indexed by Ω_i, $i = -m-1, -m, \ldots, n+1$. The dielectric constant and the Debye length are constant in each area Ω_i, denoted as ε_i and λ_i, a source charge q_s at $\mathbf{x}_s$ is inside Ω_0. Denoting the electric potential in Ω_i as Φ_i, in layer Ω_0, Φ_0 satisfies the Poisson equation [46],

$$\Delta\Phi_0(\mathbf{x}, \mathbf{x}_s) = -\frac{4\pi q_s}{\varepsilon_0}\delta(\mathbf{x} - \mathbf{x}_s). \tag{30}$$

Meanwhile, for area Ω_i, $i \neq 0$, Φ_i satisfies the linearized Poisson-Boltzmann equation [2],

$$\Delta\Phi_i - \lambda_i^2\Phi_i = 0. \tag{31}$$

Analogously, Φ_0 can be rewritten as a sum of the Coulombic contribution $\Phi_{coul} = q_s/\varepsilon_0|\mathbf{x} - \mathbf{x}_s|$ and a reaction potential Φ_{rf}. The following expansions hold,

$$\Phi_{coul}(\mathbf{x}, \mathbf{x}_s) = \int_0^{+\infty}\int_0^{+\infty} d\alpha d\beta \cos\alpha(x - x_s)\cos\beta(y - y_s)\frac{2q_s}{\varepsilon_0\pi\gamma}e^{-\gamma|z - z_s|}, \tag{32}$$

$$\Phi_{rf}(\mathbf{x}, \mathbf{x}_s) = \int_0^{+\infty}\int_0^{+\infty} d\alpha d\beta \cos\alpha(x - x_s)\cos\beta(y - y_s)[A_0 e^{\gamma z} + B_0 e^{-\gamma z}], \tag{33}$$

$$\begin{aligned}\Phi_i(\mathbf{x}, \mathbf{x}_s) = &\int_0^{+\infty}\int_0^{+\infty} d\alpha d\beta \cos\alpha(x - x_s)\cos\beta(y - y_s)\\ &\times [A_i e^{\sqrt{\gamma^2+\lambda_i^2}z} + B_i e^{-\sqrt{\gamma^2+\lambda_i^2}z}],\\ i \neq 0, \qquad &B_{-m-1} = 0, \qquad A_{n+1} = 0.\end{aligned} \tag{34}$$

Suppose that the surface Γ_i locates at $z = il$, $i = -m-1, -m, \ldots, n+1$, l is the thickness of the layer Ω_0. At each surface Γ_i, two interface conditions hold,

$$\Phi_{i-1} = \Phi_i, \quad \varepsilon_{i-1}\frac{\partial\Phi_{i-1}}{\partial z} = \varepsilon_i\frac{\partial\Phi_i}{\partial z}, \quad \text{on } \Gamma_i. \tag{35}$$

Substituting the boundary conditions (35) into the expansions yields a linear system for the coefficients A_i and B_i,

$$
\begin{cases}
A_{-1} + B_{-1} = \frac{2q_s}{\varepsilon_0 \pi \gamma} e^{-\gamma z_s} + A_0 + B_0, \\
\varepsilon_{-1}\sqrt{\gamma^2 + \lambda_{-1}^2}(A_{-1} - B_{-1}) = \frac{2q_s}{\pi} e^{-\gamma z_s} + \varepsilon_0 \gamma A_0 - \varepsilon_0 \gamma B_0, \\
A_1 e^{\sqrt{\gamma^2+\lambda_1^2} l} + B_1 e^{-\sqrt{\gamma^2+\lambda_1^2} l} = \frac{2q_s}{\varepsilon_0 \pi \gamma} e^{-\gamma(l - z_s)} + A_0 e^{\gamma l} + B_0 e^{-\gamma l}, \\
\varepsilon_1 \sqrt{\gamma^2 + \lambda_1^2}\left(A_1 e^{\sqrt{\gamma^2+\lambda_1^2} l} - B_1 e^{-\sqrt{\gamma^2+\lambda_1^2} l}\right) = \frac{-2q_s}{\pi} e^{-\gamma(l - z_s)} + \varepsilon_0 \gamma A_0 e^{\gamma l} - \varepsilon_0 \gamma B_0 e^{-\gamma l}, \\
A_{i-1} e^{il\sqrt{\gamma^2+\lambda_{i-1}^2}} + B_{i-1} e^{-il\sqrt{\gamma^2+\lambda_{i-1}^2}} = A_i e^{il\sqrt{\gamma^2+\lambda_i^2}} + B_i e^{-il\sqrt{\gamma^2+\lambda_i^2}}, \\
\varepsilon_{i-1}\sqrt{\gamma^2 + \lambda_{i-1}^2}\left(A_{i-1} e^{il\sqrt{\gamma^2+\lambda_{i-1}^2}} - B_{i-1} e^{-il\sqrt{\gamma^2+\lambda_{i-1}^2}}\right) \\
\quad = \varepsilon_i \sqrt{\gamma^2 + \lambda_i^2}\left(A_i e^{il\sqrt{\gamma^2+\lambda_i^2}} - B_i e^{-il\sqrt{\gamma^2+\lambda_i^2}}\right), \\
A_{n+1} = 0, \quad B_{-m-1} = 0, \quad i = -m, -m+1, \ldots, -1, \text{ and } 2, 3, \ldots, n.
\end{cases}
$$

Solving this linear system would give the desired expansion for each Φ_i.

References

1. Honig, B., Nicholls, A.: Classical electrostatics in biology and chemistry. Science **268**, 1144–1149 (1995)
2. Fogolari, F., Brigo, A., Molinari, H.: The Poisson-Boltzmann equation for biomolecular electrostatics: A tool for structural biology. J. Mol. Biol. **15**, 377–392 (2002)
3. Baker, N.A.: Improving implicit solvent simulations: A Poisson-centric view. Curr. Opin. Struct. Biol. **15**, 137–143 (2005)
4. Koehl, P.: Electrostatics calculations: latest methodological advances. Curr. Opin. Struct. Biol. **16**, 142–151 (2006)
5. Wang, J., Tan, C., Tan, Y.H., Lu, Q., Luo, R.: Poisson-Boltzmann solvents in molecular dynamics simulations. Commun. Comput. Phys. **3**, 1010–1031 (2008)
6. Hill, T.L.: An Introduction to Statistical Thermodynamics. Dover, New York (1986)
7. Schlick, T.: Molecular Modeling and Simulation: An Interdisciplinary Guide. Springer, Berlin (2002)
8. Fraenkel, D.: Simplified electrostatic model for the thermodynamic excess potentials of binary strong electrolyte solutions with size-dissimilar ions. Mol. Phys. **108**(11), 1435–1466 (2010)
9. Stell, G., Joslin, C.G.: The Donnan equilibrium: a theoretical study of the effects of interionic forces. Biophys. J. **50**(5), 855–859 (1986)
10. Torrie, G.M., Valleau, J.P.: Electrical double layers. 4. Limitations of the Gouy-Chapman theory. J. Phys. Chem. **86**, 3251–3257 (1982)
11. Zemaitis, J.F. Jr., Clark, D.M., Rafal, M., Scrivner, N.C.: Handbook of Aqueous Electrolyte Thermodynamics. Design Institute for Physical Property Data, American Institute of Chemical Engineers, New York (1986)
12. Kjellander, R., Marčelja, S.: Correlation and image charge effects in electric double layers. Chem. Phys. Lett. **112**, 49–53 (1984)
13. Levin, Y.: Electrostatic corrections: from plasma to biology. Rep. Prog. Phys. **65**, 1577–1632 (2002)
14. Eisenberg, B., Hyon, Y., Liu, C.: Energy variational analysis of ions in water and channels: Field theory for primitive models of complex ionic fluids. J. Chem. Phys. **133**, 104104 (2010)
15. French, R.H., Parsegian, V.A., Podgornik, R., Rajter, R.F., Jagota, A., Luo, J., Asthagiri, D., Chaudhury, M.K., Chiang, Y.-m., Granick, S., Kalinin, S., Kardar, M., Kjellander, R., Langreth, D.C., Lewis, J., Lustig, S., Wesolowski, D., Wettlaufer, J.S., Ching, W.-Y., Finnis, M., Houlihan, F., von Lilienfeld, O.A., van Oss, C.J., Zemb, T.: Long range interactions in nanoscale science. Rev. Mod. Phys. **82**(2), 1887–1944 (2010)
16. Warshel, A.: A microscopic model for calculations of chemical processes in aqueous solutions. Chem. Phys. Lett. **55**, 454–458 (1978)

17. King, G., Warshel, A.: A surface constrained all-atom solvent model for effective simulations of polar solutions. J. Chem. Phys. **91**, 3647–3661 (1989)
18. Beglov, D., Roux, B.: Finite representation of an infinite bulk system: Solvent boundary potential for computer simulations. J. Chem. Phys. **100**, 9050–9063 (1994)
19. Alper, H., Levy, R.M.: Dielectric and thermodynamic response of a generalized reaction field model for liquid state simulations. J. Chem. Phys. **99**, 9847–9852 (1993)
20. Okur, A., Simmerling, C.: Hybrid explicit/implicit solvation methods. Annu. Rep. Comput. Chem. **2**, 97–109 (2006)
21. Lin, Y., Baumketner, A., Deng, S., Xu, Z., Jacobs, D., Cai, W.: An image-based reaction field method for electrostatic interactions in molecular dynamics simulations of aqueous solutions. J. Chem. Phys. **131**, 154103 (2009)
22. Xu, Z., Cai, W.: Fast analytical methods for macroscopic electrostatic models in biomolecular simulations. SIAM Rev. **53**, 683–720 (2011)
23. Kirkwood, J.G.: Theory of solutions of molecules containing widely separated charges with special applications to zwitterions. J. Chem. Phys. **2**, 351–361 (1934)
24. Tanford, C., Kirkwood, J.G.: Theory of protein titration curves. I. General equations for impenetrable spheres. J. Am. Chem. Soc. **79**, 5333–5339 (1957)
25. Friedman, H.L.: Image approximation to the reaction field. Mol. Phys. **29**, 1533–1543 (1975)
26. Abagyan, R., Totrov, M.: Biased probability Monte Carlo conformational searches and electrostatic calculations for peptides and proteins. J. Mol. Biol. **235**, 983–1002 (1994)
27. Lindell, I.V.: Electrostatic image theory for the dielectric sphere. Radio Sci. **27**, 1–8 (1992)
28. Greengard, L., Rokhlin, V.: A fast algorithm for particle simulations. J. Comput. Phys. **73**, 325–348 (1987)
29. Greengard, L.: The Rapid Evaluation of Potential Fields in Particle Systems. MIT Press, Cambridge (1987)
30. Cai, W., Deng, S., Jacobs, D.: Extending the fast multipole method to charges inside or outside a dielectric sphere. J. Comput. Phys. **223**, 846–864 (2007)
31. Deng, S., Cai, W.: Discrete image approximations of ionic solvent induced reaction field to charges. Commun. Comput. Phys. **2**, 1007–1026 (2007)
32. Xu, Z., Deng, S., Cai, W.: Image charge approximations of reaction fields in solvents with arbitrary ionic strength. J. Comput. Phys. **228**, 2092–2099 (2009)
33. Qin, P., Xu, Z., Cai, W., Jacobs, D.: Image charge methods for a three-dielectric-layer hybrid solvation model of biomolecules. Commun. Comput. Phys. **6**, 955–977 (2009)
34. Lin, Y., Baumketner, A., Song, W., Deng, S., Jacobs, D., Cai, W.: Ionic solvation studied by image-charge reaction field method. J. Chem. Phys. **134**, 044105 (2011)
35. Xu, Z., Cai, W., Cheng, X.: Image charge method for reaction fields in a hybrid ion-channel model. Commun. Comput. Phys. **9**, 1056–1070 (2011)
36. Cui, S.T.: Electrostatic potential in cylindrical dielectric media using the image charge method. Mol. Phys. **104**, 2993–3001 (2006)
37. Boda, D., Gillespie, D., Nonner, W., Henderson, D., Eisenberg, B.: Computing induced charges in inhomogeneous dielectric media: application in a Monte Carlo simulation of complex ionic systems. Phys. Rev. E, Stat. Nonlinear Soft Matter Phys. **69**(4 Pt 2), 046702 (2004)
38. Cheng, M.H., Coalson, R.D.: An accurate and efficient empirical approach for calculating the dielectric self-energy and ion-ion pair potential in continuum models of biological ion channels. J. Phys. Chem. B **109**(1), 488–498 (2005)
39. Bardhan, J.P., Eisenberg, R.S., Gillespie, D.: Discretization of the induced-charge boundary integral equation. Phys. Rev. E, Stat. Nonlinear Soft Matter Phys. **80**(1), 011906 (2009)
40. Levitt, D.G.: Modeling of ion channels. J. Gen. Physiol. **113**, 789–794 (1999)
41. Tieleman, D.P., Biggin, P.C., Smith, G.R., Sansom, M.S.P.: Simulation approaches to ion channel structure-function relationships. Q. Rev. Biophys. **34**, 473–561 (2001)
42. Roux, B., Allen, T., Berneche, S., Im, W.: Theoretical and computational models of biological ion channels. Q. Rev. Biophys. **37**, 15–103 (2004)
43. Hille, B.: Ionic Channels of Excitable Membranes. Sinauer Associates, Sunderland (1992)
44. Eisenberg, B.: Crowded charges in ion channels. Adv. Chem. Phys. **148**, 77–223 (2012)
45. Yang, P.K., Liaw, S.H., Lim, C.: Representing an infinite solvent system with a rectangular finite system using image charges. J. Phys. Chem. B **106**, 2973–2982 (2002)
46. Jackson, J.D.: Classical Electrodynamics, 3rd edn. Wiley, New York (2001)
47. Sommerfeld, A.: Partial Differential Equations in Physics. Academic Press, New York (1949)
48. Chew, W.C.: Waves and Fields in Inhomogeneous Media. Van Nostrand, New York (1990)
49. Neumann, C.: Hydrodynamische untersuchungen: Nebst einem anhange uber die probleme der elektrostatik und der magnetischen induktion, pp. 279–282. Teubner, Leipzig (1883)

50. Lindell, I.V.: Application of the image concept in electromagnetism. In: Stone, W.R. (ed.) The Review of Radio Science 1990–1992, pp. 107–126. Oxford University Press, Oxford (1993)
51. Norris, W.T.: Charge images in a dielectric sphere. IEE Proc. Sci. Meas. Technol. **142**, 142–150 (1995)
52. Prony, R.: Essai experimental et analytique. J. Éc. Polytech. **1**, 24–76 (1795)
53. Weiss, L., McDonough, R.N.: Prony's method, z-transforms, and Padé approximation. SIAM Rev. **5**, 145–149 (1963)
54. Im, W., Beglov, D., Roux, B.: Continuum solvation model: Computation of electrostatic forces from numerical solutions to the Poisson-Boltzmann equation. Comput. Phys. Commun. **111**, 59–75 (1998)